Structural basis for antibody cross-neutralization of dengue and Zika viruses

Nicholas K. Hurlburt[1], Jay Lubow[1], Leslie Goo,[1*] Marie Pancera[1]

[1]Vaccine and Infectious Disease Division, Fred Hutchinson Cancer Center, Seattle, Washington, USA.

*Current address: Vaccine Company, Inc., South San Francisco, California, USA

Abstract

Safe and effective vaccines against co-circulating mosquito-borne orthoflaviviruses such as Zika virus (ZikV) and the four serotypes of dengue virus (DenV1-4) must elicit broadly neutralizing antibodies (bnAbs) to prevent the risk of enhancement of infection by non-neutralizing antibodies. We recently discovered new orthoflavivirus-directed bnAbs, including F25.S02, which neutralizes DenV1-4 and ZikV with comparable or superior potency to the previously characterized E dimer epitope (EDE) bnAbs. Mutagenesis studies of viral envelope proteins showed that the epitope specificity of F25.S02 is distinct from EDE1 bnAbs. Here, we used cryoEM and X-ray crystallography to understand the basis of cross-neutralization of F25.S02 at the molecular level. We obtained a ~4.2 Å cryoEM structure of F25.S02 Fab bound to a stabilized DenV3 soluble E protein dimer and a 2.3 Å crystal structure of F25.S02 Fab bound to ZikV soluble E protein dimer. Like previously described EDE1 bnAbs, the structural epitope of F25.S02 is at the E dimer interface, encompassing predominantly conserved regions in domain II, including the fusion loop. However, unlike EDE1 bnAbs, F25.S02 binding is almost entirely dependent on the heavy chain and is shifted slightly away from the dimer symmetry axis. Our findings emphasize the importance of this cross-neutralizing site of vulnerability for DenV and ZikV that can facilitate rational design of vaccines and therapeutics.

Introduction

Orthoflaviviruses are arthropod-borne, enveloped RNA viruses that can cause symptoms ranging from a self-limiting fever to potentially fatal hemorrhagic or neuroinvasive disease for which there is no treatment beyond supportive care. Many orthoflaviviruses are emerging threats to global health: the four DenV serotypes (DenV1-4) infect an estimated 390 million people annually[1]; ZikV emerged outside of Asia and Africa for the first time in 2007 and was repeatedly introduced into the Americas in 2014-2015, leading to considerable morbidity[2]. The ability of orthoflaviviruses to rapidly emerge from relative obscurity to serious public health threats combined with the geographical expansion of mosquito vectors[3], further facilitated by climate change [4], underscores the importance of effective clinical interventions.

The envelope (E) protein of orthoflaviviruses, including DenV1-4 and ZikV, is a key structural protein involved in viral entry and membrane fusion, and is the target of antibodies [5]. The soluble form of this protein (sE) retains many of the antigenic properties of the native virion-associated E protein [6]. While structurally conserved across DenV1–4 and ZikV, variations in sE can influence virus-specific interactions with host antibodies and receptors, impacting cross-reactivity and immune protection [7].

The complex antibody response to co-circulating and antigenically related orthoflaviviruses presents a major challenge for vaccine development. Specifically, the presence of cross-reactive, non-neutralizing antibodies to E protein from a prior exposure to ZikV or a given DenV serotype predicts the risk of severe disease following secondary exposure to a different DenV serotype[8, 9] - a process known as antibody-dependent enhancement (ADE) of infection. To minimize the risk of ADE, a safe and effective vaccine must elicit antibodies that simultaneously neutralize DenV1-4, and ideally, ZikV. Despite decades of research, ADE-related safety concerns ultimately derailed the widespread use of the first licensed DenV vaccine[10]. This unfortunate outcome eroded public confidence in vaccines in general[11]. Thus, although many successful vaccines have been developed without first knowing the specific targets of the antibodies they

elicited, such empirical approaches to developing DenV vaccines have been insufficient. A rational approach to vaccine design to limit the elicitation of non-neutralizing antibodies is needed and this requires improving our fundamental understanding of how orthoflavivirus bnAbs recognize their targets. A few bnAbs that can potently neutralize DenV1-4 and in some cases, ZikV, have been isolated from infected individuals. The most well-characterized bnAbs target an envelope-dimer epitope (EDE) spanning both E protein protomers within the dimer subunit as defined by X-ray crystallography and cryo-electron microscopy (cryo-EM)[12, 13]. There are two subclasses of EDE bnAbs, of which EDE1 but not EDE2 can potently neutralize ZikV in addition to DenV1-4[14]. Until recently, SIgN-3C was the only known naturally occurring, cross-neutralizing antibody outside the EDE1 class[15]. Unlike EDE antibodies, which target an *intra*-dimer epitope, SIgN-3C binds an epitope at the *inter*-dimer interface[16], as determined by cryo-EM. Recently, we identified F25.S02, another naturally occurring bnAb with broad and potent cross-neutralization of DenV1-4 and ZikV [17]. Mutational and neutralization analysis showed that the F25.S02 epitope was distinct from the EDE1 bnAb C10 [17]. Here, we determined the binding mechanism of F25.S02 to DenV3 sE dimer by cryoEM and to ZikV sE dimer using X-ray crystallography. The structures revealed that F25.S02 differs in its mode of binding compared to other cross-neutralizing EDE1 antibodies. Our results can ultimately guide structure-based vaccine design, the promise of which is best exemplified by the recently approved vaccine for respiratory syncytial virus[18].

Results

F25.S02 binds a highly conserved patch on DenV3 sE

We previously showed that F25.S02 had the highest neutralization potency against DenV3[17]. We expressed and purified a previously described stabilized sE protein dimers (DenV3 sE sc30)[19] and a His-tagged antigen binding fragment (Fab) of F25.S02. We formed a stable complex as indicated by a monodisperse peak by size-exclusion chromatography (SEC) (**Supplementary Fig. 1a**) and used this

complex to obtain a cryoEM reconstruction to 4.2 Å resolution (**Fig. 1a, Supplementary Fig. 2, Supplementary Table 1**)**.** The map revealed the sE dimer with two Fabs bound at the envelope dimer interface, similar to what has been shown with previously identified EDE1 antibodies [14, 20]. F25.S02 interacts with domain I and III of one protomer and domain II and fusion loop of the other protomer (**Fig. 1A**). The local resolution of the F25.S02 for most of the binding site is around 3.5 Å, increasing the confidence in sidechain assignment (**Supplementary Fig. 2d, e**). F25.S02 binds DenV3 with a total buried surface area (BSA) of ~1,157 $Å^2$ with ~1,010 $Å^2$ from the heavy chain (HC) and ~147 $Å^2$ from the light chain (LC). Thus, nearly 87% of the BSA comes from the HC (**Fig. 1B**). The F25.S02 binding site is a highly conserved patch on the E protein among all DenV serotypes and ZikV (**Fig. 1C**) as shown by mapping the surface with a conservation score generated by the Consurf server[21].

The cryoEM map shows clear density for the first N-acetylglucosamine (GlcNAc) of the N67 glycan (**Supplementary Fig. 3a**) and two GlcNAc and one mannose of the N153 glycan (**Supplementary Fig. 3b**); both glycans are conserved among DenV serotypes. F25.S02 does not contact the glycan at N67 but interacts with the glycan at N153. This was unexpected because we previously showed that mutations at either N153 or T155 to remove the glycan increased F25.S02 neutralization potency against DenV2 [17]. To determine if the glycan was needed for DenV3 recognition, we removed the glycan by mutating threonine 155 to alanine (T155A) and tested binding of F25.S02 to DenV3 sE sc30 T155A by biolayer interferometry (BLI). The BLI data showed that the T155A mutation had no effect on F25.S02 Fab binding to DenV3 sE sc30, indicating that the N153 glycan is not necessary for binding (**Supplementary Fig. 1b**) even though it contributes ~213 $Å^2$ of buried surface area (18% of the total BSA for DenV3).

F25.S02 binds ZikV sE at the E dimer interface

As F25.S02 cross-neutralized DenV and ZikV, we next determined its structure bound to ZikV to understand the basis of its cross-reactivity. The wildtype (WT) ZikV sE dimer showed high affinity binding

97 for F25.S02 (**Supplementary Fig. 1c**). To increase yield for structural studies, we co-expressed ZikV sE WT
98 with F25.S02 Fab and obtained enough complex for crystallization experiments. The purified complex was
99 confirmed by SEC to be sE dimer with two Fabs bound (**Supplementary Fig. 1d**). Well diffracting crystals
100 were obtained, and an X-ray structure was determined to 2.3 Å resolution (**Fig. 2a, Supplementary Table**
101 **2**). The crystal had a $P4_12_12$ space group with an sE dimer and two Fabs in the asymmetric unit (ASU). The
102 structure was solved by molecular replacement with R_{work} and R_{free} of 0.225 and 0.274, respectively
103 (**Supplementary Table 2**). Like in the DenV3 structure, the ZikV structure shows that the F25.S02 epitope
104 is mostly HC dependent, accounting for ~77% of the total BSA (**Fig2. b, f**). The total BSA of F25.S02 on ZikV
105 is ~1,464 $Å^2$ with ~1,130 $Å^2$ from the HC and ~334 $Å^2$ from the LC. All three CDRHs are involved in binding
106 but only the CDRL2 is involved in binding with single residues in framework region (FR) 2 and FR3 having
107 minor contributions (**Fig. 2f**).
108 The majority of the interactions between F25.S02 and ZikV sE are located on domain II and the fusion loop
109 of protomer A (**Fig. 2c**). The CDRH2 sits in a shallow pocket formed by the fusion loop, the β-strand *b* and
110 the *ij* loop of domain II. The CDRH3 contains a one turn α-helix and sits on the surface formed by β-strand
111 *b* and the fusion loop. Glu_{73HC} in FR3 of the HC forms a H-bond with $Arg_{252ZikV}$ in domain II while Ser_{74HC} of
112 FR3 interacts with $Asp_{278ZikV}$ of protomer B. The CDRH1 of F25.S02 interacts with the 150 loop of domain I
113 of protomer B, which contains the N154 glycan (**Fig. 2d**), that is equivalent to N153 in DenV (of note, ZikV
114 lacks the glycan at position 67 present in DenV). Interactions between F25.S02 LC and ZikV sE are all
115 located on domain III with the CDRL2 forming three H-bonds with domain III of protomer B. The HC forms
116 a single interaction with domain III with Leu_{100EHC} sitting between Lys_{316} of one protomer and the fusion
117 loop of the other (**Fig. 2e**).
118 The N154 glycan is well resolved in the electron density, unlike in many other structures of antibodies
119 bound to orthoflavivirus sE proteins [14, 20]. For both protomers, electron density can clearly be seen up
120 to the branching mannose, with electron density resolving the α1-3 and α1-6 mannose in protomer A

121 while only the α1-3 mannose is seen with protomer B (**Fig. 2d, Supplementary Fig. 3c, d**). Interestingly,
122 there are numerous interactions and H-bonds between F25.S02 and the N154 glycan. The first two N-
123 terminal residues of the HC interact with the first and second GlcNAc and Arg_{94HC} forms a hydrogen bond
124 with the C3 hydroxyl of the first GlcNAc. Additionally, Lys_{42LC} and Lys_{45LC} of the LC interact with α1-3
125 mannose with Lys_{45LC} forming a H-bond with the C4 hydroxyl (**Fig. 2d**). In total, the interactions with the
126 N154 glycan account for ~23% of the total BSA (350 $Å^2$) between F25.S02 and ZikV sE (**Fig. 2f**). Due to poor
127 expression levels of ZikV sE WT, we were not able to produce enough to confirm if the removal of the
128 glycan would affect F25.S02 binding affinity but it was previously shown that removal of the N154 glycan
129 increased the neutralization potency of F25.S02 against ZikV [22], indicating that the glycan is not required
130 for binding or neutralization.
131
132 **F25.S02 binds ZikV sE in a nearly identical manner as DenV3**
133 The residues of F25.S02 that interact with ZikV sE and DenV3 sE dimers are highly similar and most V-gene
134 interactions are germline encoded, with only Met_{51HC} being mutated from Ile (**Fig. 2f**). An alignment of the
135 sE dimer of the ZikV and DenV3-F25.S02 bound structures shows good overlap with a root mean square
136 deviation (RMSD) of 3.94 Å over 775 paired α carbons (Cα) (**Fig. 3a**). DenV3-bound F25.S02 Fv is shifted
137 outward slightly relative to the ZikV-bound F25.S02 Fv, but this is mostly due to the slight difference in
138 conformations of the sE proteins. When aligning the Fv domains of one of the F25.S02 Fabs in each
139 structure, the overall RMSD is 1.02 Å over 234 paired Cα (**Fig. 3b**). In this alignment, the fusion loop and
140 bound portions of domain II almost completely overlap. If you remove the interactions with the
141 N153/N154 glycan from the BSA data, F25.S01 binds DenV3 sE with 85% HC and ZikV sE with 82% HC. The
142 contact with the glycan in ZikV is 222 $Å^2$ from the HC and 128 $Å^2$ from the LC, while in DenV3, the HC and
143 LC contact with an area of 201 and 13 $Å^2$, respectively. The LC binding contribution to the glycans in the
144 ZikV bound structure explains the difference between the 87% vs 77% overall BSA contribution of the HC

145 to Denv3 versus ZikV. In all, F25.S02 primarily utilizes its HC to bind to the highly conserved fusion loop of
146 DenV1-4 and ZikV. The light chain interactions are primarily with main chain atoms of ZikV sE that are not
147 highly conserved, the only side chain H-bond is from Arg_{54LC} to $Glu_{370ZikV}$ in ZikV and a similar residue (Glu_{370}
148 in DenV1 and 3, Asp_{370} in DenV2 and Asn in DenV4) is present in DenV1-4 that would be capable of forming
149 this interaction (**Fig. 3c**).
150

151 **F25.S02 binds a similar but distinct epitope to EDE1 antibodies**

152 We compared the binding mechanism of F25.S02 to two EDE1 bnAbs, C8[14] and C10[20], which also
153 cross-neutralize DenV1-4 and ZikV. An alignment of the ZikV-bound C8 and C10 to ZikV-bound F25.S02
154 structure shows that both C8 and C10 have a larger footprint on domain II and bind closer to the dimer
155 symmetry axis (**Fig. 4a**). Both C8 and C10 were shown to interact with N67 glycan on DenV (absent in ZikV)
156 that is not required for binding or neutralization [14, 20]. F25.S02 does not interact with this glycan on
157 DenV3 (**Fig. 3b**). For both C8 and C10, the CDRL3 occupies the position of the F25.S02 CDRH3 (**Fig. 4b**),
158 highlighting this shift towards the center of the sE dimer. An alignment of the Fv domains of C8 and C10
159 to F25.S02 further shows the distinction between the binding mechanisms. When C8 is aligned with
160 F25.S02, the two Fv domains align with an RMSD of 2.73 Å over 227 paired Cα. The C8-bound sE dimer is
161 shifted toward the interior relative to the F25.S02-bound sE dimer (**Fig. 4c, top**). When C10 is aligned with
162 F25.S02, the Fv domains have an RMSD of 2.50 Å over 233 paired Cα. Not only is the sE dimer shifted to
163 the center relative to F25.S02 bound ZikV sE, but the angle of approach is rotated about 20° (**Fig. 4c,**
164 **bottom**). In comparison, C8 and C10 have an RMSD of 2.01 Å over 229 paired Cα, highlighting that F25.S02
165 is more distinct from C8 and C10 than they are from each other. The difference in binding is further shown
166 by comparing the footprint on the ZikV sE dimer (**Fig. 4d**). Both C8 and C10 bind with a nearly equal split
167 of BSA between HC and LC. C8 has a HC contribution of 46% and C10 has a HC contribution of 50% to ZikV
168 sE, while F25.S02 is 82% HC binding by BSA (**Fig. 4f**).

169 Another cross-neutralizing bnAb against DenV1-4 and ZikV is SIgN-3C, which differs from EDE1 antibodies
170 by making both intra- and inter-dimer contacts [16]. When compared to F25.S02, SIgN-3C binding
171 footprint on ZikV sE is shifted away from domain I of the intra-dimer pair and to the exterior face of the
172 adjacent dimer, interacting with both domain I and II (**Fig. 4e**). SIgN-3C binds with a similar amount of BSA
173 as F25.S02 and is also mostly HC dependent (**Fig. 4f**), but its footprint is shifted to make the inter-dimer
174 interaction (**Fig. 4d, bottom**). In all, F25.S02 binds a similar epitope as EDE1 antibodies but employs a
175 distinct method of binding that is HC dependent and is confined to intra-dimer interactions, unlike SIgN-
176 3C.
177
178 **Discussion**
179 Our structural analysis of F25.S02, a potent cross-neutralizing antibody against ZikV and the four DenV
180 serotypes, reveals a common heavy chain-dominant binding mechanism to a highly conserved patch on
181 the E protein at the interface of the two protomers. The F25.02 epitope encompasses domain II and the
182 fusion loop of one protomer and domains I and III of the other protomer in the sE dimer. Interestingly, it
183 appears that F25.S02 can readily accommodate glycans within the epitope but is not glycan-dependent
184 for binding or neutralization. This has been observed in HIV envelope-directed antibodies where bnAbs
185 mature to accommodate glycans but are not needed for neutralization [23-25].
186
187 The main differences in binding of F25.S02 to DenV3 and ZikV are observed at the residue insertion
188 present in ZikV. First, the insertion in the domain I loop, which includes the glycan at position N153/N154
189 (DenV3/ZikV, respectively), results in $N154_{ZikV}$ being in closer proximity to the F25.S02 Fab, with its light
190 chain making additional glycan contacts as seen in that structure (**Fig. 2d and Supplementary Fig. 3**).
191 Second, the insertion in domain III (residues 359-360 in DenV3, residues 370-373 in ZikV) also contributes
192 to more interactions of ZikV sE with F25.S02 light chain compared to DenV3 (**Fig. 2e**).

193 The analysis suggests F25.S02 crosslinks the dimer, which would inhibit conformational changes required
194 for viral fusion with the host membrane. This mechanism of neutralization has been reported for EDE1
195 bnAbs, which also cross-neutralize DenV1-4 and ZikV [14, 20]. However, as we only obtained structures
196 with the sE dimer, we cannot conclude if F25.S02 would induce a similar conformational change as EDE1
197 antibodies on viral particles [17]. We presently do not observe the asymmetric conformation reported
198 before of the sE dimer and thus cannot readily explain the differences in affinity and potency observed
199 for F25.S02 with ZikV and DenV1-4 [20]. In addition, we did not obtain structures of F25.S02 with the other
200 DenV serotypes and could not come up with a plausible explanation for the reported differences in
201 neutralization potency across serotypes by modeling the interactions at the residue level [20].

202 Further structural studies with the virions would need to be done to determine how F25.S02 binds to E
203 protein in its native form on the viral particle. We nevertheless modeled F25.S02 Fab binding to the virus,
204 by aligning our F25.S02-ZikV sE crystal structure on the whole virus cryoEM structure of ZikV (PDBid 6CO8)
205 [26] (**Fig. 5a**). The alignment indicated F25.S02 Fab could bind on the particle in every position on the
206 three-dimer raft (**Fig. 5c**), as well as all positions around the 3-fold symmetry axis (**Fig. 5b**) without steric
207 clashes. There could be a potential clash of F25.S02 light chain at the 5-fold symmetry axis (5f position)
208 (**Fig. 5d**) that could have an impact on the avidity of binding of F25.S02 antibody as seen for other EDE1
209 antibodies.[20].
210

211 While F25.S02's epitope is similar to previously reported cross-neutralizing EDE-antibodies, its binding
212 mode is distinct as 1) it uses predominantly heavy chain recognition, 2) its binding is shifted away from
213 the 2-fold symmetry axis of the dimer and N67 glycan in DenV3, and 3) most of its interactions are
214 mediated by germline residues [14, 20]. With SIgN-3C and F25.S02, the interactions to ZikV E protein use
215 a similar footprint area and both utilize a predominantly heavy chain mode of binding, but F25.S02 lacks

216 the inter-dimer interactions that are necessary for SIgN-3C recognition [16]. Thus, F25.S02 binds a similar
217 site with a distinct mode of binding and could be a distinct class of cross-neutralizing antibody.
218
219 The structural information that F25.S02 binds a highly conserved epitope present on both ZikV and DenV,
220 and that its mode of binding is primarily heavy chain dependent with little affinity maturation required
221 for broad neutralization makes its epitope an interesting target for rational or computational vaccine
222 design that would elicit broadly neutralizing antibodies.
223
224
225
226
227
228
229
230
231
232
233
234
235
236
237
238
239

240 **Methods**

241 **Fab expression and purification**

242 The gene encoding the variable region of the heavy chain of F25.S02 was cloned into a vector with a
243 human CH1 domain with a C-terminal his-tag using the Platinum SuperFi II DNA polymerase
244 (ThermoFisher, 12368010) and the In-Fusion cloning system (Takara Bio, 638948). The Fab was expressed
245 in HEK293E (RRID:CVCL_HF20) cells at 1×10^6 cells/mL using a total of 500 µg DNA per liter of culture (1:1
246 ratio of HC-to-LC DNA). PEI was used as the transfection reagent at a ratio of 4:1 PEI-to-DNA. Culture was
247 harvested after 6 days and Fab was purified from cultural supernatant using His60 Ni Superflow resin
248 (Takara Bio). Fab was eluted from column using buffer containing 50 mM Tris, pH 7.5, 300 mM NaCl, and
249 150 mM Imidazole. F25.S02 Fab was further purified using a HiLoad 16/600 Superdex 200 size exclusion
250 column (Cytivia) on an AKTApure system (GE Biosciences) into a buffer containing 5 mM HEPES, 150 mM
251 NaCl, pH 7.5.

252

253 **sE protein expression**

254 Plasmids for WT and stabilized sE proteins were kindly provided by Brian Kulhman (University of North
255 Carolina at Chapel Hill) [19]. sE proteins were expressed in Expi293F cells according to manufacturer's
256 protocol (ThermoFisher, A14635). Cultures were harvested 6 days after transfection and cleared
257 supernatant was incubated with His60 Ni Superflow resin (Takara Bio, 635660). sE protein was eluted from
258 column using buffer containing 50 mM Tris, pH 7.5, 300 mM NaCl, and 300 mM imidazole. For structural
259 studies, protein was further purified by size exclusion chromatography (SEC) using a HiLoad 16/600
260 Superdex 200 column (Cytiva) or a Superdex 200 Increase 10/300 column (Cytiva) on a AKTApure system
261 (GE Biosciences). SEC peak corresponding to dimer was kept and concentrated using a 10K MWCO Amicon
262 Ultra Centrifugal Filter (Millipore Sigma, UFC901024).

263 Plasmid for DenV3 sE sc30 T155A was made via site-directed mutagenesis using the Platinum SuperFi II
264 DNA polymerase (ThermoFisher, 12368010) and DenV3 sE sc30 T155A expressed and purified as above.
265
266 **sE+F25.S02 complex formation**
267 For DenV3 sE sc30, sE protein was mixed with F25.S02 Fab in a 1:2.5 dimer-to-Fab ratio for 2 hours at 4°C
268 with nutation. Complex was purified on a HiLoad 16/600 Superdex 200 column (Cytiva) and fractions
269 corresponding to complex were pooled and concentrated to OD_{280}=8. Complex was divided into 20 µL
270 aliquots, flash frozen in LN2, and stored at -80°C.
271 For the ZikV sE WT + F25.S02 Fab complex, the plasmid for ZikV sE WT was mutated to remove the 8x His-
272 tag using the In-Fusion cloning system (Takara Bio, 638948). Complex was expressed in Expi293F cells
273 according to manufacturer's protocol using a plasmid DNA ratio of 2:1:1 sE-to-HC-to-LC. Culture was
274 harvested 6 days after transfection and complex was purified from cultural supernatant using His60 Ni
275 Superflow resin (Takara Bio). Protein was eluted using buffer containing 50 mM Tris, pH 7.5, 300 mM NaCl,
276 and 300 mM Imidazole. Complex was further purified using a HiLoad 16/600 Superdex 200 size exclusion
277 column (Cytivia) on an AKTApure system (GE Biosciences) into a buffer containing 5 mM HEPES, 150 mM
278 NaCl, pH 7.5. Fractions corresponding to complex were pooled and concentrated to OD_{280}=25, divided into
279 50 µL aliquots and flash frozen in LN2. All aliquots were stored at -80°C.
280
281 **Biolayer interferometry**
282 F25.S02 binding was measured using biolayer interferometry on an Octet 96 Red instrument (ForteBio)
283 using FAB2G biosensors (Sartorius). F25.S02 Fab was diluted to 10 µg/mL in kinetics buffer (1× PBS, 0.01%
284 Tween 20, 0.01% BSA and 0.005% NaN3, pH 7.4). Each sE protein was diluted to 1 µM in kinetics buffer.
285 Fab was loaded onto biosensor until a threshold of 1.0 nm shift was reached. After loading, biosensors
286 were placed in kinetics buffer for 60 sec for a baseline reading. Biosensors were then immersed in analyte

287 for 300 sec in the association phase, followed by 300 sec in the dissociation phase in kinetics buffer. The
288 background signal from a biosensor loaded with Fab but with no analyte was subtracted from each loaded
289 biosensor.
290
291 **CryoEM sample preparation**
292 DenV3 sE sc30+F25.S02 Fab complex was thawed and diluted to OD_{280}=5. Just prior to grid preparation,
293 complex was mixed with 0.1% Tween20 to a final concentration of 0.25 CMC (0.5 µL of 0.1% Tween20 into
294 20 µL of complex). 3 µL of complex was loaded onto UltrAuFoil R1.2/1.3 300mesh grids (Ted Pella) and
295 manually blotted. Another 3 µL was loaded onto grid and vitrified on a Vitrobot Mark IV (ThermoFisher)
296 with a blot force of 2, blot time of 4 sec at 4°C and 100% humidity before plunging into liquid ethane.
297
298 **CryoEM data collection and processing**
299 Data was collected on a 200 kV Glacios microscope (ThermoFisher) with a K3 direct electron detector
300 (Gatan) at a magnification of 36,000x (1.122 Å per pixel) using SerialEM [27]. A total of 1,195 movies were
301 collected with 100 exposures over 6 sec. Motion correction was performed using Warp [28] and processed
302 using cryoSPARC (V4.5) [29]. Initial 2D templates were generated through multiple rounds of 2D
303 classification. Using 2D templates, particles were re-extracted using template picker. A total of ~2 million
304 particles were extracted and after 3 rounds of 2D classification, 111,111 particles were used for Ab-initio
305 reconstruction without symmetry. The reconstruction was refined using homogenous refinement
306 followed by non-uniform refinement [30] with C2 symmetry. Local refinement was performed using a
307 mask to exclude the Fc domain of F25.S02. The FSC curve suggested heterogeneity in the particles and a
308 3D classification was used to separate particles into two classes. Following homogeneous refinement, one
309 class showed better quality and was further refined with local refinement with a mask to exclude the Fc

310 domain and 64,110 particles. The resolution was estimated to be 4.16 Å per the gold standard $FSC_{0.143}$.
311 Local resolution was estimated based on gold standard $FSC_{0.143}$ and is shown in **Supplementary Fig. 2**.
312

313 **CryoEM model building and refinement**

314 The model of DenV3 sE protomer from PDBid 7A3P [20] was used as the initial model and a model of
315 F25.S02 Fab was generated by AlphaFold3 [31]. Both models were docked into the cryoEM map using
316 ChimeraX (v1.9) [32]. Model building was completed using Coot (v0.9.8.1) [33] and an initial refinement
317 was run using Phenix (v1.21) real_space_refinement [34]. Further refinement was performed using
318 ISOLDE [35] in ChimeraX [32] and Coot [33]. Data collection and refinement statistics are summarized in
319 **Supplementary Table 1**. Structural figures were generated using ChimeraX and the conserved residue
320 map was generated using the ConSurf web server [21] with the E protein sequences from the reference
321 strains of DenV1-4 and ZikV. BSA data was determined using the PDBePISA server [36].
322

323 **Crystallization and structure determination**

324 Initial crystallization screening was performed by sitting-drop vapor diffusion using ProPlex crystallization
325 screen (Molecular Dimensions) and an NT8 drop setting robot (Formulatrix) at a complex concentration
326 of OD_{280}=15. Initial crystals grew in drop F5 (0.1 M Tris, pH 8.0, 0.1 M NaCl, 8% w/v PEG 20K). Well
327 diffracting crystals were grown via hanging-drop vapor diffusion in 0.1 M Tris, pH 8.0, 0.1 M NaCl, 5% w/v
328 PEG 20K and were frozen with 40% PEG 200 as a cryoprotectant. Diffraction data was collected at
329 Advanced Light Source beamline 5.0.3 at 12.7 keV. The dataset was processed using XDS [37] and AIMLESS
330 [38] to a resolution of 2.30 Å. Initial phases were solved by molecular replacement using Phaser in Phenix
331 [34] with a search model of ZikV sE protomer from PDBid 5JHM [39] and the AlphaFold3 [31] model of
332 F25.S02 Fab split into Fv and CH1/CL domains. Model building was completed using Coot [33] and
333 refinement was performed in Phenix. Additional model refinement was done using ISOLDE [35] in

ChimeraX [32]. Data collection and refinement statistics are summarized in **Supplementary Table 2**. BSA data was determined using the PDBePISA server [36].

358 **References**

359 1. Bhatt S, Gething PW, Brady OJ, Messina JP, Farlow AW, Moyes CL, et al. The global distribution
360 and burden of dengue. Nature. 2013;496(7446):504-7. Epub 20130407. doi: 10.1038/nature12060.
361 PubMed PMID: 23563266; PubMed Central PMCID: PMCPMC3651993.
362 2. Weaver SC, Costa F, Garcia-Blanco MA, Ko AI, Ribeiro GS, Saade G, et al. Zika virus: History,
363 emergence, biology, and prospects for control. Antiviral Res. 2016;130:69-80. Epub 20160318. doi:
364 10.1016/j.antiviral.2016.03.010. PubMed PMID: 26996139; PubMed Central PMCID: PMCPMC4851879.
365 3. Kraemer MUG, Reiner RC, Jr., Brady OJ, Messina JP, Gilbert M, Pigott DM, et al. Past and future
366 spread of the arbovirus vectors Aedes aegypti and Aedes albopictus. Nat Microbiol. 2019;4(5):854-63.
367 Epub 20190304. doi: 10.1038/s41564-019-0376-y. PubMed PMID: 30833735; PubMed Central PMCID:
368 PMCPMC6522366.
369 4. Iwamura T, Guzman-Holst A, Murray KA. Accelerating invasion potential of disease vector Aedes
370 aegypti under climate change. Nat Commun. 2020;11(1):2130. Epub 20200501. doi: 10.1038/s41467-
371 020-16010-4. PubMed PMID: 32358588; PubMed Central PMCID: PMCPMC7195482.
372 5. Kuhn RJ, Zhang W, Rossmann MG, Pletnev SV, Corver J, Lenches E, et al. Structure of dengue
373 virus: implications for flavivirus organization, maturation, and fusion. Cell. 2002;108(5):717-25. doi:
374 10.1016/s0092-8674(02)00660-8. PubMed PMID: 11893341; PubMed Central PMCID:
375 PMCPMC4152842.
376 6. Rey FA, Heinz FX, Mandl C, Kunz C, Harrison SC. The envelope glycoprotein from tick-borne
377 encephalitis virus at 2 A resolution. Nature. 1995;375(6529):291-8. doi: 10.1038/375291a0. PubMed
378 PMID: 7753193.
379 7. Stettler K, Beltramello M, Espinosa DA, Graham V, Cassotta A, Bianchi S, et al. Specificity, cross-
380 reactivity, and function of antibodies elicited by Zika virus infection. Science. 2016;353(6301):823-6.
381 Epub 20160714. doi: 10.1126/science.aaf8505. PubMed PMID: 27417494.
382 8. Katzelnick LC, Gresh L, Halloran ME, Mercado JC, Kuan G, Gordon A, et al. Antibody-dependent
383 enhancement of severe dengue disease in humans. Science. 2017;358(6365):929-32. Epub 20171102.
384 doi: 10.1126/science.aan6836. PubMed PMID: 29097492; PubMed Central PMCID: PMCPMC5858873.
385 9. Katzelnick LC, Narvaez C, Arguello S, Lopez Mercado B, Collado D, Ampie O, et al. Zika virus
386 infection enhances future risk of severe dengue disease. Science. 2020;369(6507):1123-8. doi:
387 10.1126/science.abb6143. PubMed PMID: 32855339; PubMed Central PMCID: PMCPMC8274975.
388 10. Dengue vaccine: WHO position paper, September 2018 - Recommendations. Vaccine.
389 2019;37(35):4848-9. Epub 20181110. doi: 10.1016/j.vaccine.2018.09.063. PubMed PMID: 30424888.
390 11. Larson HJ, Hartigan-Go K, de Figueiredo A. Vaccine confidence plummets in the Philippines
391 following dengue vaccine scare: why it matters to pandemic preparedness. Hum Vaccin Immunother.
392 2019;15(3):625-7. Epub 20181012. doi: 10.1080/21645515.2018.1522468. PubMed PMID: 30309284;
393 PubMed Central PMCID: PMCPMC6605722.
394 12. Dejnirattisai W, Wongwiwat W, Supasa S, Zhang X, Dai X, Rouvinski A, et al. A new class of highly
395 potent, broadly neutralizing antibodies isolated from viremic patients infected with dengue virus. Nat
396 Immunol. 2015;16(2):170-7. Epub 20141215. doi: 10.1038/ni.3058. PubMed PMID: 25501631; PubMed
397 Central PMCID: PMCPMC4445969.
398 13. Rouvinski A, Guardado-Calvo P, Barba-Spaeth G, Duquerroy S, Vaney MC, Kikuti CM, et al.
399 Recognition determinants of broadly neutralizing human antibodies against dengue viruses. Nature.
400 2015;520(7545):109-13. Epub 20150112. doi: 10.1038/nature14130. PubMed PMID: 25581790.
401 14. Barba-Spaeth G, Dejnirattisai W, Rouvinski A, Vaney MC, Medits I, Sharma A, et al. Structural
402 basis of potent Zika-dengue virus antibody cross-neutralization. Nature. 2016;536(7614):48-53. Epub
403 20160623. doi: 10.1038/nature18938. PubMed PMID: 27338953.

404 15. Kam YW, Lee CY, Teo TH, Howland SW, Amrun SN, Lum FM, et al. Cross-reactive dengue human
405 monoclonal antibody prevents severe pathologies and death from Zika virus infections. JCI Insight.
406 2017;2(8). Epub 20170420. doi: 10.1172/jci.insight.92428. PubMed PMID: 28422757; PubMed Central
407 PMCID: PMCPMC5396524.
408 16. Zhang S, Loy T, Ng TS, Lim XN, Chew SV, Tan TY, et al. A Human Antibody Neutralizes Different
409 Flaviviruses by Using Different Mechanisms. Cell Rep. 2020;31(4):107584. doi:
410 10.1016/j.celrep.2020.107584. PubMed PMID: 32348755.
411 17. Lubow J, Levoir LM, Ralph DK, Belmont L, Contreras M, Cartwright-Acar CH, et al. Single B cell
412 transcriptomics identifies multiple isotypes of broadly neutralizing antibodies against flaviviruses. PLOS
413 Pathogens. 2023;19(10):e1011722. doi: 10.1371/journal.ppat.1011722.
414 18. FDA Approves First Respiratory Syncytial Virus (RSV) Vaccine [Internet]. U.S. Food and Drug
415 Administration; 2023. Available from: https://www.fda.gov/news-events/press-announcements/fda-
416 approves-first-respiratory-syncytial-virus-rsv-vaccine
417 19. Phan TTN, Hvasta MG, Kudlacek ST, Thiono DJ, Tripathy A, Nicely NI, et al. A conserved set of
418 mutations for stabilizing soluble envelope protein dimers from dengue and Zika viruses to advance the
419 development of subunit vaccines. J Biol Chem. 2022;298(7):102079. Epub 20220526. doi:
420 10.1016/j.jbc.2022.102079. PubMed PMID: 35643320; PubMed Central PMCID: PMCPMC9249817.
421 20. Sharma A, Zhang X, Dejnirattisai W, Dai X, Gong D, Wongwiwat W, et al. The epitope
422 arrangement on flavivirus particles contributes to Mab C10's extraordinary neutralization breadth across
423 Zika and dengue viruses. Cell. 2021;184(25):6052-66 e18. Epub 20211130. doi:
424 10.1016/j.cell.2021.11.010. PubMed PMID: 34852239; PubMed Central PMCID: PMCPMC8724787.
425 21. Yariv B, Yariv E, Kessel A, Masrati G, Chorin AB, Martz E, et al. Using evolutionary data to make
426 sense of macromolecules with a "face-lifted" ConSurf. Protein Sci. 2023;32(3):e4582. doi:
427 10.1002/pro.4582. PubMed PMID: 36718848; PubMed Central PMCID: PMCPMC9942591.
428 22. Contreras M, Stuart JB, Levoir LM, Belmont L, Goo L. Defining the impact of flavivirus envelope
429 protein glycosylation site mutations on sensitivity to broadly neutralizing antibodies. mBio.
430 2024;15(2):e0304823. Epub 20240109. doi: 10.1128/mbio.03048-23. PubMed PMID: 38193697;
431 PubMed Central PMCID: PMCPMC10865826.
432 23. Zhou T, Georgiev I, Wu X, Yang ZY, Dai K, Finzi A, et al. Structural basis for broad and potent
433 neutralization of HIV-1 by antibody VRC01. Science. 2010;329(5993):811-7. Epub 20100708. doi:
434 10.1126/science.1192819. PubMed PMID: 20616231; PubMed Central PMCID: PMCPMC2981354.
435 24. Parks KR, MacCamy AJ, Trichka J, Gray M, Weidle C, Borst AJ, et al. Overcoming Steric
436 Restrictions of VRC01 HIV-1 Neutralizing Antibodies through Immunization. Cell Rep. 2019;29(10):3060-
437 72 e7. doi: 10.1016/j.celrep.2019.10.071. PubMed PMID: 31801073; PubMed Central PMCID:
438 PMCPMC6936959.
439 25. Umotoy J, Bagaya BS, Joyce C, Schiffner T, Menis S, Saye-Francisco KL, et al. Rapid and Focused
440 Maturation of a VRC01-Class HIV Broadly Neutralizing Antibody Lineage Involves Both Binding and
441 Accommodation of the N276-Glycan. Immunity. 2019;51(1):141-54 e6. doi:
442 10.1016/j.immuni.2019.06.004. PubMed PMID: 31315032; PubMed Central PMCID: PMCPMC6642152.
443 26. Sevvana M, Long F, Miller AS, Klose T, Buda G, Sun L, et al. Refinement and Analysis of the
444 Mature Zika Virus Cryo-EM Structure at 3.1 A Resolution. Structure. 2018;26(9):1169-77 e3. Epub
445 20180626. doi: 10.1016/j.str.2018.05.006. PubMed PMID: 29958768; PubMed Central PMCID:
446 PMCPMC6125166.
447 27. Mastronarde DN. Automated electron microscope tomography using robust prediction of
448 specimen movements. J Struct Biol. 2005;152(1):36-51. doi: 10.1016/j.jsb.2005.07.007. PubMed PMID:
449 16182563.

450 28. Tegunov D, Cramer P. Real-time cryo-electron microscopy data preprocessing with Warp. Nat
451 Methods. 2019;16(11):1146-52. Epub 20191007. doi: 10.1038/s41592-019-0580-y. PubMed PMID:
452 31591575; PubMed Central PMCID: PMCPMC6858868.
453 29. Punjani A, Rubinstein JL, Fleet DJ, Brubaker MA. cryoSPARC: algorithms for rapid unsupervised
454 cryo-EM structure determination. Nat Methods. 2017;14(3):290-6. Epub 20170206. doi:
455 10.1038/nmeth.4169. PubMed PMID: 28165473.
456 30. Punjani A, Zhang H, Fleet DJ. Non-uniform refinement: adaptive regularization improves single-
457 particle cryo-EM reconstruction. Nat Methods. 2020;17(12):1214-21. Epub 20201130. doi:
458 10.1038/s41592-020-00990-8. PubMed PMID: 33257830.
459 31. Abramson J, Adler J, Dunger J, Evans R, Green T, Pritzel A, et al. Accurate structure prediction of
460 biomolecular interactions with AlphaFold 3. Nature. 2024;630(8016):493-500. Epub 20240508. doi:
461 10.1038/s41586-024-07487-w. PubMed PMID: 38718835; PubMed Central PMCID: PMCPMC11168924.
462 32. Meng EC, Goddard TD, Pettersen EF, Couch GS, Pearson ZJ, Morris JH, et al. UCSF ChimeraX:
463 Tools for structure building and analysis. Protein Sci. 2023;32(11):e4792. doi: 10.1002/pro.4792.
464 PubMed PMID: 37774136; PubMed Central PMCID: PMCPMC10588335.
465 33. Emsley P, Lohkamp B, Scott WG, Cowtan K. Features and development of Coot. Acta Crystallogr
466 D Biol Crystallogr. 2010;66(Pt 4):486-501. Epub 20100324. doi: 10.1107/S0907444910007493. PubMed
467 PMID: 20383002; PubMed Central PMCID: PMCPMC2852313.
468 34. Liebschner D, Afonine PV, Baker ML, Bunkoczi G, Chen VB, Croll TI, et al. Macromolecular
469 structure determination using X-rays, neutrons and electrons: recent developments in Phenix. Acta
470 Crystallogr D Struct Biol. 2019;75(Pt 10):861-77. Epub 20191002. doi: 10.1107/S2059798319011471.
471 PubMed PMID: 31588918; PubMed Central PMCID: PMCPMC6778852.
472 35. Croll TI. ISOLDE: a physically realistic environment for model building into low-resolution
473 electron-density maps. Acta Crystallogr D Struct Biol. 2018;74(Pt 6):519-30. Epub 20180411. doi:
474 10.1107/S2059798318002425. PubMed PMID: 29872003; PubMed Central PMCID: PMCPMC6096486.
475 36. Krissinel E, Henrick K. Inference of macromolecular assemblies from crystalline state. J Mol Biol.
476 2007;372(3):774-97. Epub 20070513. doi: 10.1016/j.jmb.2007.05.022. PubMed PMID: 17681537.
477 37. Kabsch W. Xds. Acta Crystallogr D Biol Crystallogr. 2010;66(Pt 2):125-32. Epub 20100122. doi:
478 10.1107/S0907444909047337. PubMed PMID: 20124692; PubMed Central PMCID: PMCPMC2815665.
479 38. Agirre J, Atanasova M, Bagdonas H, Ballard CB, Basle A, Beilsten-Edmands J, et al. The CCP4
480 suite: integrative software for macromolecular crystallography. Acta Crystallogr D Struct Biol. 2023;79(Pt
481 6):449-61. Epub 20230530. doi: 10.1107/S2059798323003595. PubMed PMID: 37259835; PubMed
482 Central PMCID: PMCPMC10233625.
483 39. Dai L, Song J, Lu X, Deng YQ, Musyoki AM, Cheng H, et al. Structures of the Zika Virus Envelope
484 Protein and Its Complex with a Flavivirus Broadly Protective Antibody. Cell Host Microbe.
485 2016;19(5):696-704. Epub 20160502. doi: 10.1016/j.chom.2016.04.013. PubMed PMID: 27158114.

486

487

488

489

490

491

492 **Acknowledgements**

493 We thank Dr. Brian Kuhlman for providing DenV3 and ZikV sE plasmids. We thank the J. B. Pendleton
494 Charitable Trust for its generous support of Formulatrix robotic instruments. This work was supported by
495 a Fred Hutch Vaccine and Infectious Disease Division (VIDD) Initiative grant. Electron microscopy data
496 were generated using the Fred Hutchinson Cancer Center Electron Microscopy Shared Resource. The
497 EMSR is supported in part by the Cancer Center Support Grant P30 CA015704. The Berkeley Center for
498 Structural Biology is supported in part by the Howard Hughes Medical Institute. The Advanced Light
499 Source is a Department of Energy Office of Science User Facility under Contract No. DE-AC02-05CH11231.
500 The ALS-ENABLE beamlines are supported in part by the National Institutes of Health, National Institute
501 of General Medical Sciences, grant P30 GM124169.

502

503 **Contributions**

504 N.K.H., J.L., L.G., and M.P. conceived the project. N.K.H., J.L., L.G., and M.P. designed the experiments.
505 N.K.H performed the cloning, expressed and purified the proteins, formed the complexes, collected and
506 processed the cryoEM data, and built and refined the model. N.K.H. crystallized the protein, collected and
507 processed the diffraction data, and solved the crystal structure. N.K.H., J.L., L.G., and M.P. analyzed and
508 discussed data. N.K.H. and M.P. wrote the original manuscript draft. N.K.H., J.L., L.G., and M.P. reviewed
509 and edited the manuscript. N.K.H., J.L., L.G. and M.P. secured funding for the project.

510

511 **Competing Interests**

512 J.L. and L.G. are inventors on a patent application filed by Fred Hutchinson Cancer Center relating to
513 F25.S02. The other authors have no competing interests.

514

515

516 **Figures**

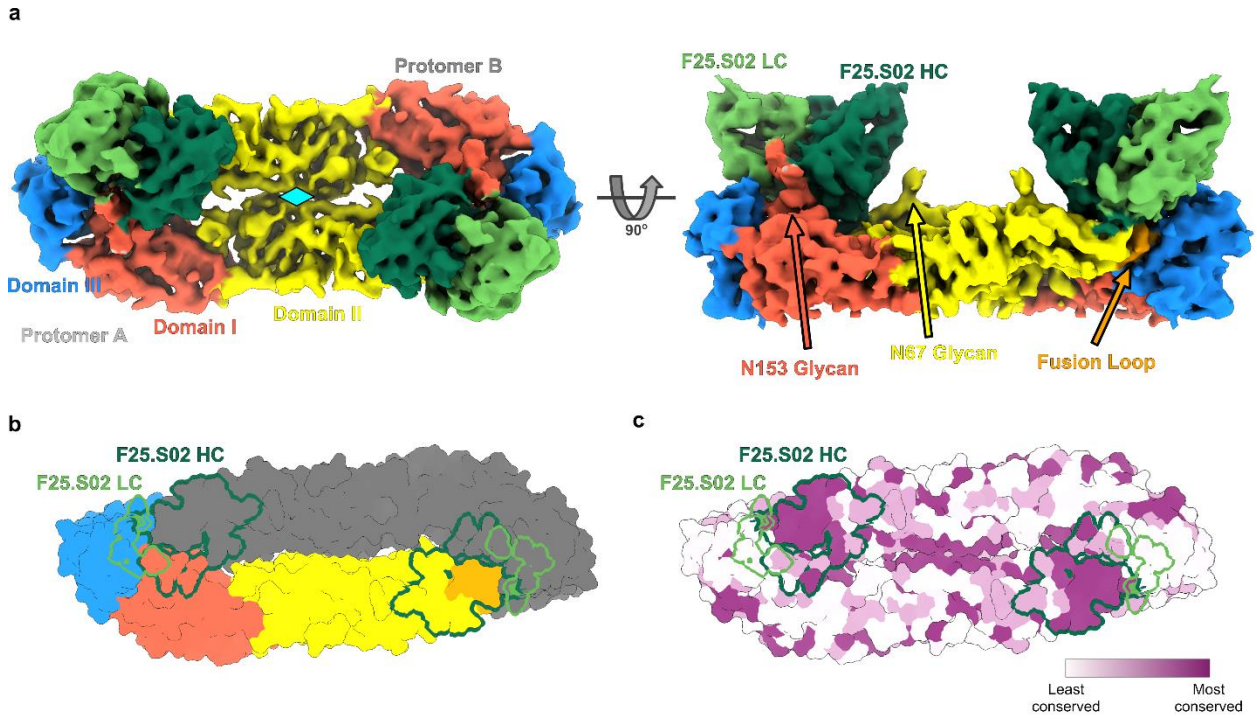

517

518 **Figure 1. CryoEM structure of F25.S02 bound to DenV3 sE** a) The cryoEM map of F25.S02 Fab bound to
519 DenV3 sE sc30. The map is colored to highlight the domains of the sE protein with the glycans labeled and
520 their locations shown. F25.S02 Fv is shown in dark green for the heavy chain and light green for the light
521 chain. Cyan diamond represents the 2-fold symmetry axis of the dimer. b) Model of DenV3 sE sc30 dimer
522 shown in surface representation with one protomer colored to show the domains and the other in gray.
523 The binding footprint of F25.S02 is highlighted with the heavy chain binding site in dark green and the
524 light chain in light green. c) The same model from b) but colored to show conservation of residues across
525 DenV serotypes and ZikV sE proteins. Coloring was generated using the ConSurf server.

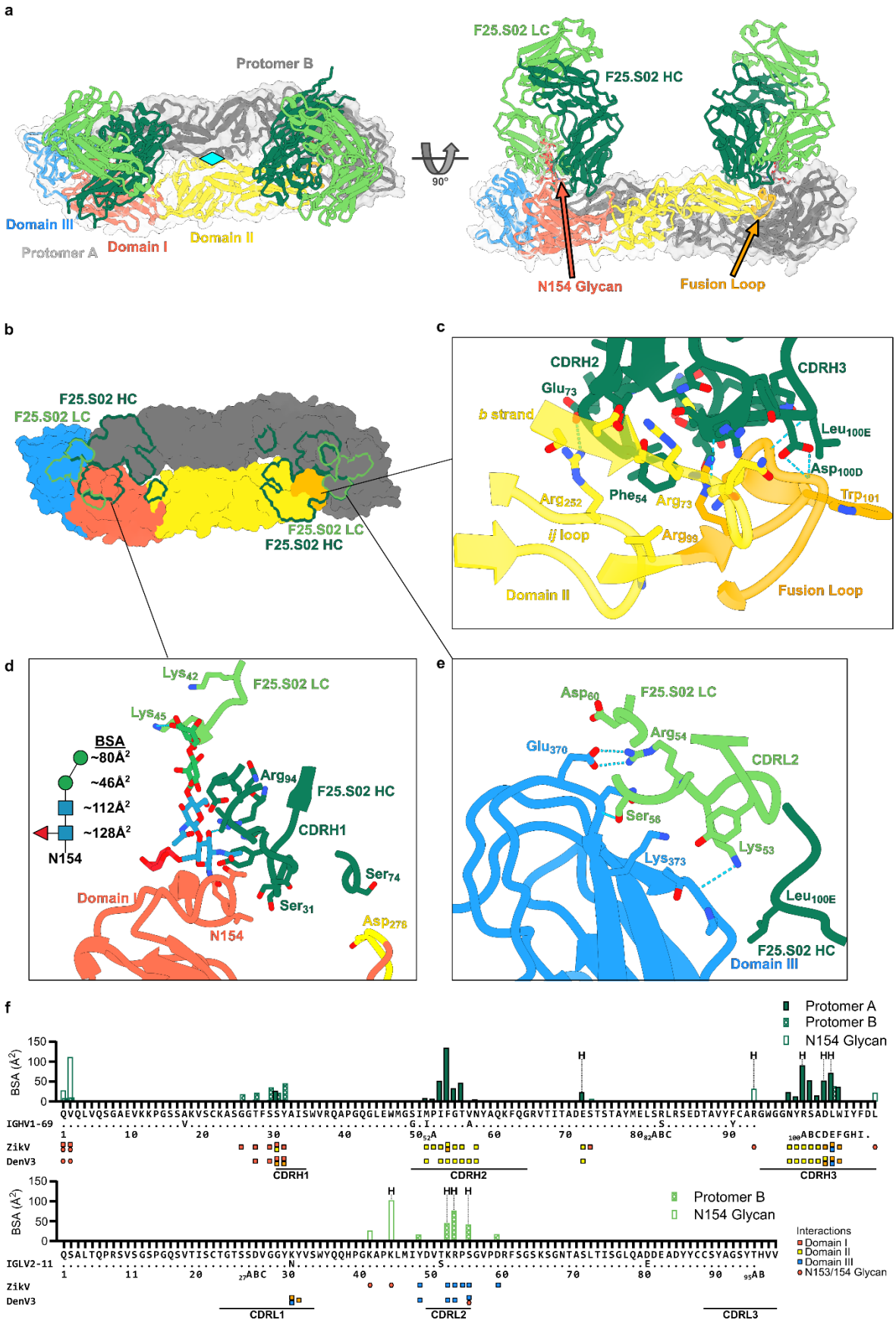
a
Protomer B
Domain III
Protomer A
Domain I
Domain II
F25.S02 LC
F25.S02 HC
90°
N154 Glycan
Fusion Loop
b
F25.S02 HC
F25.S02 LC
F25.S02 LC
F25.S02 HC
c
CDRH2
CDRH3
Glu73
b strand
Leu100E
Asp100D
Trp101
Arg252
Phe54
Arg73
jj loop
Arg99
Domain II
Fusion Loop
d
Lys42
F25.S02 LC
Lys45
BSA
~80Å2
~46Å2
~112Å2
~128Å2
N154
Arg94
F25.S02 HC
CDRH1
Ser74
Domain
Ser31
N154
Asp278
e
Asp60
F25.S02 LC
Arg54
Glu370
CDRL2
Ser56
Lys53
Lys373
Leu100E
F25.S02 HC
Domain III
f
Protomer A
Protomer B
N154 Glycan
BSA (Å2)
IGHV1-69
ZikV
DenV3
CDRH1
CDRH2
CDRH3
Protomer B
N154 Glycan
IGLV2-11
Interactions
Domain I
Domain II
Domain III
N153/154 Glycan
CDRL1
CDRL2
CDRL3

526

527 **Figure 2. X-ray crystal structure of F25.S02 bound to ZikV sE** a) The X-ray crystal structure of F25.S02 Fab
528 bound to ZikV sE dimer is shown in cartoon representation. The sE protein includes a transparent surface
529 representation with one protomer colored to highlight domains I, II, and III and the other shown in grey.
530 F25.S02 Fab is shown in dark green for the heavy chain and light green for the light chain. Cyan diamond
531 represents the 2-fold symmetry axis of the dimer. b) Surface representation of the ZikV sE dimer with the
532 F25.S02 epitope outlined in dark green for the heavy chain and light green for the light chain. c) Zoom in
533 of the binding interactions of F25.S02 with domain II and the fusion loop. Hydrogen bonds are indicated
534 by the blue dashed lines and interacting residues are labeled and shown in sticks. d) Zoom in of the binding
535 interactions of F25.S02 with domain I and the N154 glycan. Hydrogen bonds are indicated by the blue
536 dashed lines. The diagram of the N154 glycan is shown with the amount of BSA of each carbohydrate
537 listed. Blue square represents N-acetylglucosamine, red triangle is fucose, and green circle is mannose. e)
538 Zoom in of the binding interactions of F25.S02 with domain III. Hydrogen bonds are indicated by the blue
539 dashed lines. f) BSA plot showing which residues of F25.S02 are involved in the binding to ZikV sE. The
540 germline V-genes of both heavy and light chains are shown and the CDRs are indicated. The residues
541 involved in binding to ZikV and DenV3 sE are shown and color coded to indicate which domain they
542 interact with.

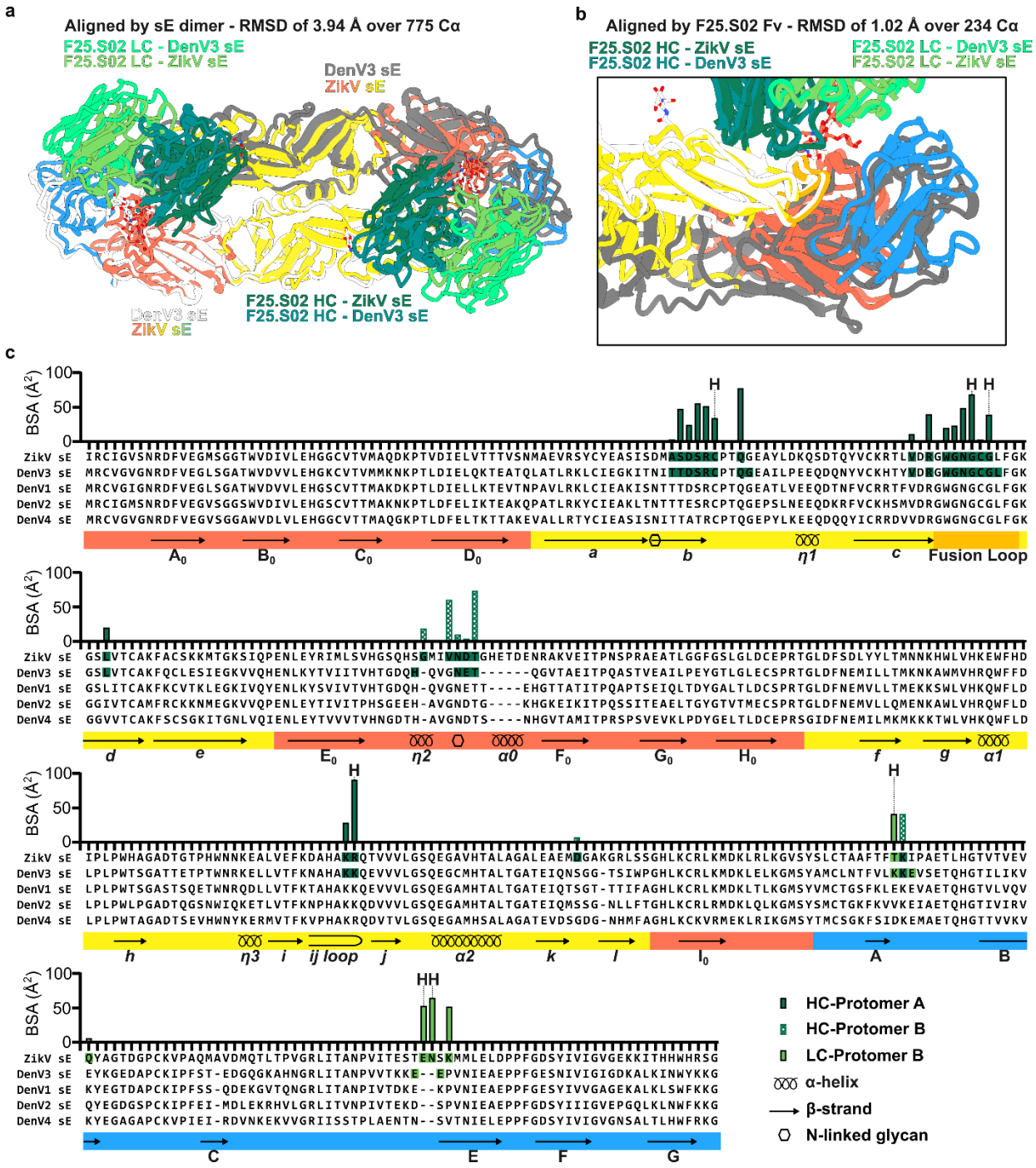

Figure 3. Comparison of F25.S02 bound to DenV3 and ZikV sE a) Alignment of ZikV and DenV3 sE structure. Alignment was made by matchmaking the sE dimer in ChimeraX. b) Alignment of ZikV and DenV3 sE structure highlighting a single Fab-dimer interaction. Alignment was made by matchmaking the Fv domain of F25.S02 in ChimeraX. c) BSA plot of ZikV sE bound by F25.S02 with an alignment of DenV1-4

548 sE. The DenV3 residues interacting with F25.S02 are highlighted in the alignment. The domains and fusion
549 loop are colored and the secondary structural elements of ZikV sE as well as the N-linked glycan sites are
550 shown.

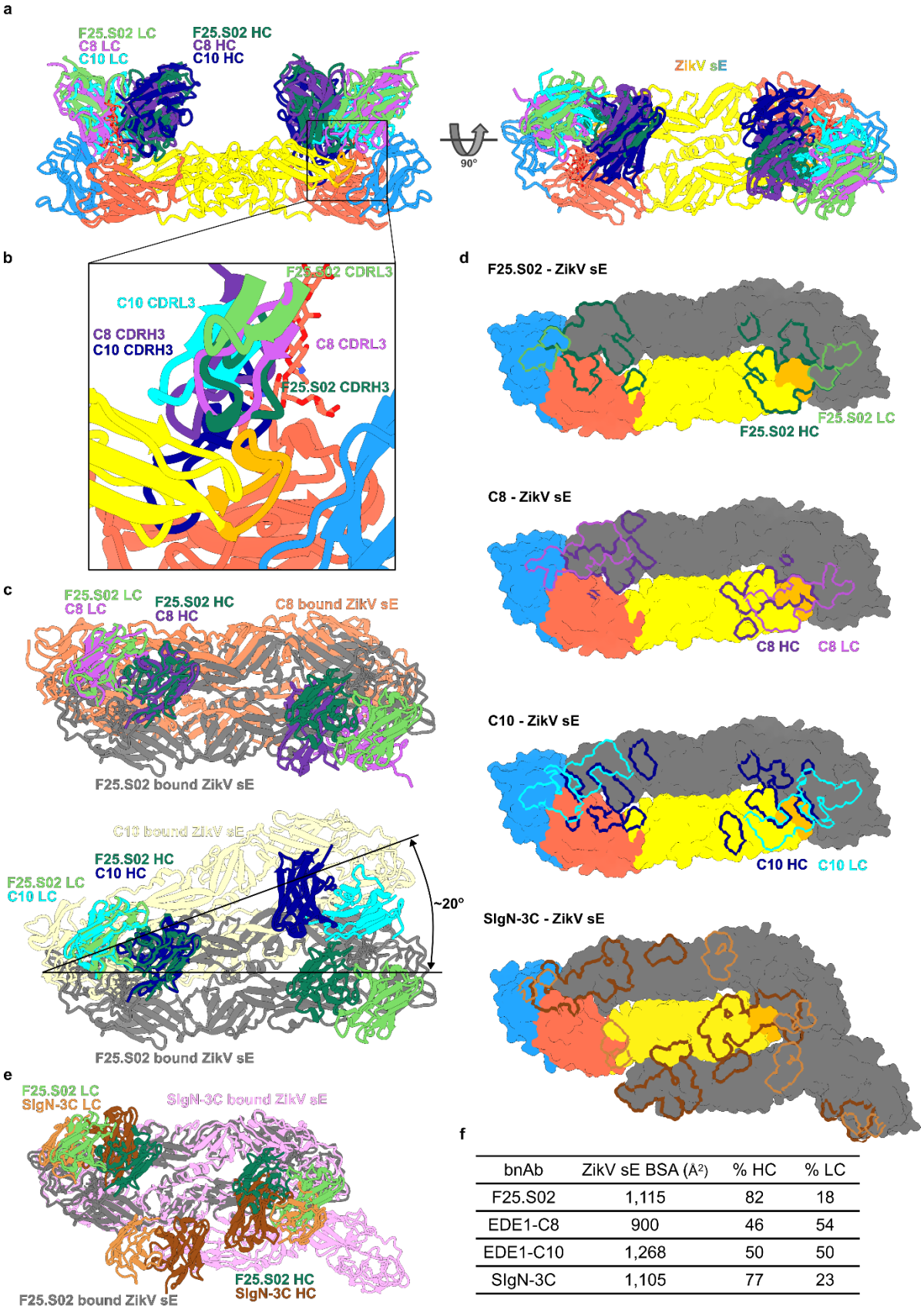

f

bnAb	ZikV sE BSA (Å²)	% HC	% LC
F25.S02	1,115	82	18
EDE1-C8	900	46	54
EDE1-C10	1,268	50	50
SIgN-3C	1,105	77	23

551

552 **Figure 4. Structural comparison of F25.S02 to other orthoflavivirus bnAb** a) Alignment of EDE1
553 antibodies, C8 and C10, bound to ZikV sE and the F25.S02 bound ZikV sE. Alignment was made by
554 matchmaking the sE dimer in ChimeraX. Only the F25.S02 bound ZikV sE is shown for simplicity. b) Zoom
555 in of the interactions of F25.S02, C8, and C10 to the fusion loop. Both C8 and C10 CDRL3 bind in the
556 location of the F25.S02 CDRH3. c) Alignment of C8 and C10 to F25.S02 by Fv domain of one Fab in the
557 dimer. Alignment of C8-ZikV sE and F25.S02-ZikV sE (top). Alignment of C10-ZikV sE and F25.S02-ZikV sE
558 (bottom). d) Surface representation of the ZikV sE dimer with epitopes of F25.S02, C8, and C10 outlined.
559 e) Alignment of F25.S02 and SIgN-3C of bound ZikV sE dimer. The alignment was made by matchmaking
560 the sE dimer in ChimeraX. F) Table showing the total BSA of each bnAb footprint on ZikV sE and the
561 respective contribution of the heavy and light chains.

562

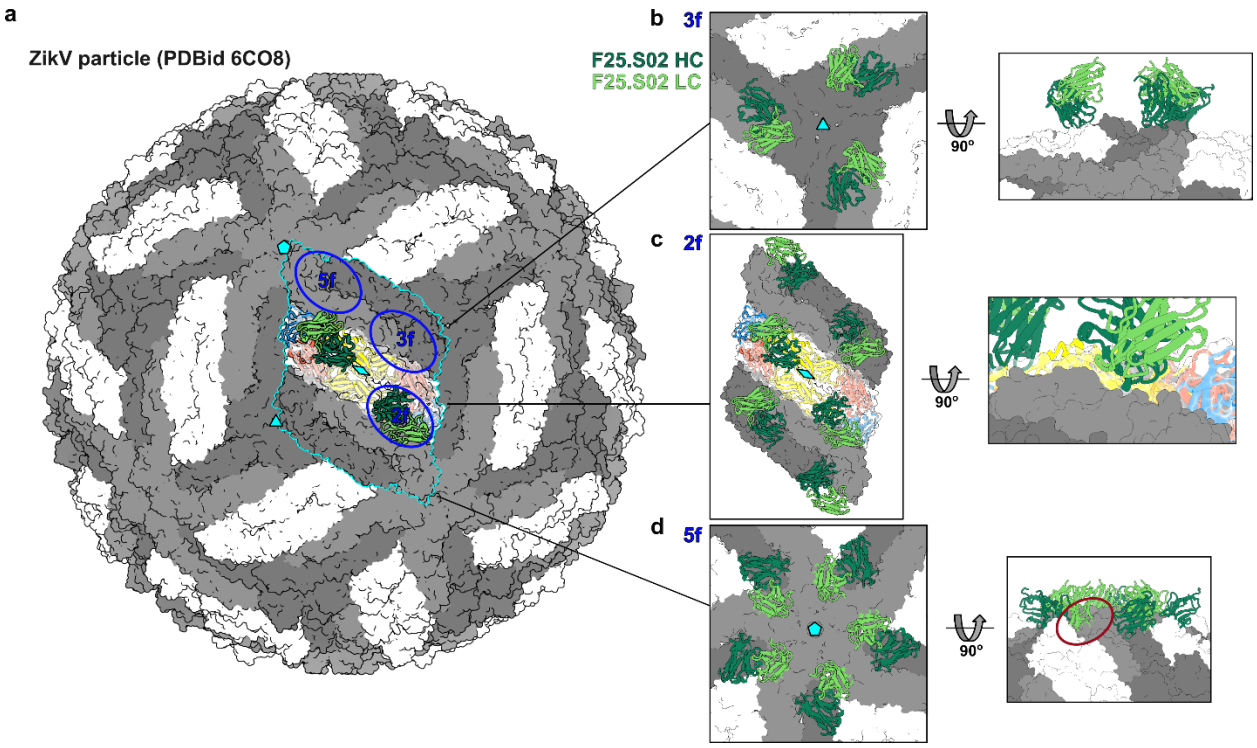

563

564

565 **Figure 5. Alignment of F25.S02 to ZikV viral particle** a) Alignment of the F25.S02-ZikV sE crystal

566 structure on the whole virus cryoEM structure of ZikV (PDBid 6CO8). The sE raft is highlighted in cyan.

567 The sE dimer 2-fold symmetry is shown by the diamond, the icosahedral 3-fold and 5-fold symmetry

568 axes are shown by the triangle and pentagon, respectively. The E protein binding sites, 2f, 3f, and 5f are

569 shown with blue circles b) Zoom in showing potential binding of F25.S02 at the 3f site. c) zoom in

570 showing potential F25.S02 binding in an E protein raft on the particle. d) Zoom in showing potential

571 binding of F25.S02 at the 5f site. Light chain would potentially clash with adjacent dimer.

572

573